JGR Space Physics

RESEARCH ARTICLE
10.1029/2021JA030089

Lobe Reconnection and Cusp-Aligned Auroral Arcs

S. E. Milan[1,2], G. E. Bower[1], J. A. Carter[1], L. J. Paxton[3], B. J. Anderson[3], and M. R. Hairston[4]

[1]School of Physics and Astronomy, University of Leicester, Leicester, UK, [2]Birkeland Centre for Space Sciences, University of Bergen, Bergen, Norway, [3]Johns Hopkins University Applied Physics Laboratory, Laurel, MD, USA, [4]William B. Hanson Center for Space Sciences, University of Texas at Dallas, Richardson, TX, USA

Key Points:

- Cusp-aligned arcs were observed for 2 days of near-zero clock angle interplanetary magnetic field following the St. Patrick's Day storm of 2013
- Arcs were produced by upwards field-aligned currents associated with vorticity within a highly structured ionospheric convection pattern
- We propose that the magnetosphere was nearly closed, but complicated lobe reconnection geometries interleaved open and closed flux

Correspondence to:
S. E. Milan,
steve.milan@le.ac.uk

Citation:
Milan, S. E., Bower, G. E., Carter, J. A., Paxton, L. J., Anderson, B. J., & Hairston, M. R. (2022). Lobe reconnection and cusp-aligned auroral arcs. *Journal of Geophysical Research: Space Physics*, *127*, e2021JA030089. https://doi.org/10.1029/2021JA030089

Received 29 OCT 2021
Accepted 25 MAY 2022

Abstract

Following the St. Patrick's Day (17 March) geomagnetic storm of 2013, the interplanetary magnetic field had near-zero clock angle for almost two days. Throughout this period multiple cusp-aligned auroral arcs formed in the polar regions; we present observations of, and provide a new explanation for, this poorly understood phenomenon. The arcs were observed by auroral imagers onboard satellites of the Defense Meteorological Satellite Program. Ionospheric flow measurements and observations of energetic particles from the same satellites show that the arcs were produced by inverted-V precipitation associated with upward field-aligned currents (FACs) at shears in the convection pattern. The large-scale convection pattern revealed by the Super Dual Auroral Radar Network and the corresponding FAC pattern observed by the Active Magnetosphere and Planetary Electrodynamics Response Experiment suggest that dual-lobe reconnection was ongoing to produce significant closure of the magnetosphere. However, we propose that once the magnetosphere became nearly closed complicated lobe reconnection geometries arose that produced interleaving of regions of open and closed magnetic flux and spatial and temporal structure in the convection pattern that evolved on timescales shorter than the orbital period of the DMSP spacecraft. This new model naturally explains many features of cusp-aligned arcs, including why they focus in from the nightside toward the cusp region.

Plain Language Summary

The geomagnetic storm that occurred on St. Patrick's Day in 2013 was followed by a period of almost two days during which the magnetic field embedded within the solar wind was pointing purely northwards, a rare occurrence. Auroral observations reveal that a series of auroral arcs formed near the geomagnetic poles which were aligned along the sunwards direction. Measurements of flows within the polar ionosphere reveal that these arcs were associated with shears in the convection pattern and electrical currents linking the magnetosphere and ionosphere. We propose a mechanism by which these flows could be produced, invoking complicated patterns of magnetic reconnection occurring at high latitudes on the dayside magnetopause. These observations shed light on the poorly understood solar wind-magnetosphere-ionosphere coupling processes that occur when the interplanetary magnetic field is directed northwards.

1. Introduction

Milan, Carter, Bower, et al. (2020) recently proposed that dual-lobe reconnection (DLR), occurring during periods of prolonged northwards interplanetary magnetic field (IMF), can close significant amounts of the previously open magnetic flux of the magnetosphere. This newly closed flux is distributed to high latitudes in the dawn and dusk sectors, producing the horse-collar auroras (HCA) morphology and giving the polar cap a teardrop shape (e.g., Elphinstone et al., 1993; Hones Jr et al., 1989; Murphree et al., 1982), and forming a low latitude boundary layer at the flanks of the magnetosphere (Lu et al., 2011; Song & Russell, 1992). In this paper we discuss what happens if this process continues until the magnetosphere approaches total closure, and the role of lobe reconnection in producing the cusp-aligned auroral arcs that appear across the polar regions during northwards-directed IMF.

Dungey's open model of the magnetosphere (Dungey, 1961), invoking magnetic reconnection at the low latitude dayside magnetopause and in the magnetotail (Figure 1a), has been highly successful in explaining many aspects of the structure and dynamics of the magnetosphere, including the excitation of magnetospheric and ionospheric convection (the typical twin-cell convection pattern), the dependence of geomagnetic activity on the orientation and strength of the IMF (Fairfield, 1967; Fairfield & Cahill, 1966), the existence of an extended magnetotail (Ness et al., 1967; Wolfe et al., 1967) and regions near the poles largely devoid of auroras (the polar caps). The extension of Dungey's picture to include time-dependent dayside and nightside reconnection rates,

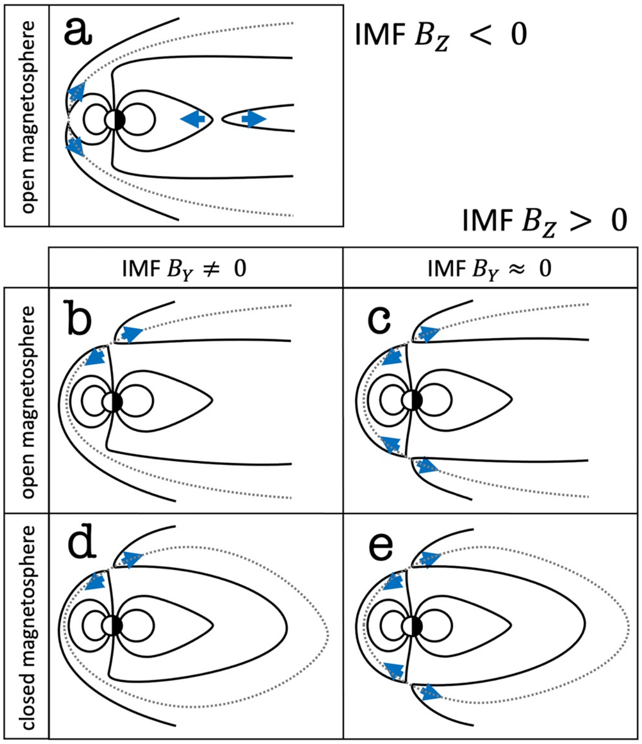

Figure 1. A schematic diagram of the reconnection geometries available for southward and northward interplanetary magnetic field (IMF). (a) Southward IMF leading to reconnection of closed magnetic flux near the subsolar magnetopause, in turn leading to magnetotail reconnection, together driving the Dungey cycle. (b) Northward IMF and single lobe reconnection (SLR) with open magnetic flux in the northern hemisphere; the open flux content of the magnetosphere is unchanged. (c) Dual lobe reconnection occurring with open lobe flux in both hemispheres; open flux is closed. (d) SLR in the northern hemisphere in a closed magnetosphere, opening magnetic flux. (e) Dual lobe reconnection in a closed magnetosphere; the magnetosphere remains closed. Adapted from Cowley (1981).

the expanding/contracting polar cap model (Cowley & Lockwood, 1992), has allowed it to incorporate phenomena such as substorms (Lockwood & Cowley, 1992; Milan et al., 2007) and geomagnetic storms (Milan et al., 2009). Day- and nightside reconnection rates can also be used to assess the open flux content and length of the magnetotail (Milan, 2004).

During northwards IMF (or NBZ) conditions distorted convection, which can include sunward flows at noon, is observed within the polar ionosphere (e.g., Chisham et al., 2004; Huang et al., 2000; Reiff & Burch, 1985), driven by the occurrence of reconnection between the IMF and the magnetic field of the magnetospheric lobes, tailward of the cusps (Cowley, 1981; Dungey, 1963). If there is a significant B_Y component during northward IMF then single lobe reconnection (SLR) occurs, that is an individual IMF field line reconnects in the northern or southern hemisphere only (Figure 1b). (Lobe reconnection may also be occurring in the opposite hemisphere, but a different IMF field line is involved.) In this case an asymmetric pattern of flows is observed, the sunward flow having a significant dawnwards or duskwards component depending on the polarity of B_Y, produced by magnetic tension forces on the newly reconnected field lines. Usually, SLR does not change the open magnetic flux content of the magnetosphere, occurring with an open lobe field line and resulting in a new open field line. On the other hand, if $B_Y \approx 0$ then DLR can occur, in which the same IMF field line reconnects in both hemispheres, producing closed field lines (Figure 1c). In this case a relatively symmetrical pattern of ionospheric flows is expected, as discussed by Milan, Carter, Bower, et al. (2020).

Under prolonged NBZ conditions the magnetotail can become unusually short (Fairfield et al., 1996) and display atypical structure and dynamics (e.g., Huang et al., 2002), suggesting that the magnetosphere is entirely closed. In this paper we discuss the possibility that this closure is caused by prolonged DLR. The role of DLR in producing partial flux closure has been investigated (Imber et al., 2006, 2007; Marcucci et al., 2008; Milan, Carter, Bower, et al., 2020), but the process is still poorly understood. However, it has been asserted on the basis of magnetospheric simulations, that in the case of purely northward IMF DLR can close the magnetosphere entirely (Figure 1e) and magnetospheric circulation goes into reverse, with sunward ionospheric flows at noon and antisunward return flows at lower latitudes (Siscoe et al., 2011; Song et al., 1999). On the other hand, if SLR occurs in a closed magnetosphere, then flux will be reopened (Figure 1d). In this paper we discuss flux closure by DLR and the complicated dynamics that are driven when the magnetosphere is (nearly) closed.

Auroral dynamics help to shine light on the complicated processes that occur under NBZ conditions (Fear, 2021; Hosokawa et al., 2020; Kullen, 2012; Zhu et al., 1997). NBZ auroral features can include a cusp spot (Carter et al., 2020; Frey et al., 2002; Milan et al., 2000b), high latitude dayside auroras or HiLDAs (Cai et al., 2021; Carter et al., 2018; Frey, 2007; Han et al., 2020; Zhang et al., 2021), and transpolar arcs (e.g., Carter et al., 2017; Cumnock & Blomberg, 2004; Cumnock et al., 2002; Fear et al., 2014; Frank et al., 1982; Kullen et al., 2002; Milan et al., 2005). Under purely NBZ conditions ($B_Y \approx 0$), when DLR is expected to occur, the polar regions can become filled with multiple sun-aligned arcs, also known as cusp-aligned arcs due to their characteristic pattern (Zhang et al., 2016), which are as yet poorly understood (e.g., Zhang et al., 2020). As they form under similar conditions, we might expect that HCA and cusp-aligned arcs are in some way related. In this paper we present observations of auroras, energetic particle precipitation, ionospheric flows, and field-aligned currents that support the suggestion that closure of the magnetosphere can occur through DLR, producing HCA, and that this is also related to the formation of cusp-aligned arcs.

2. Observations

We employ observations of the auroras, ionospheric flows, and precipitating particles in both northern and southern hemispheres (NH and SH) from the Defense Meteorological Satellite Program (DMSP) F16, F17, and F18 satellites in sun-synchronous orbits near an altitude of 850 km. The Ion Driftmeter (IDM) component of the Special Sensors–Ions, Electrons, and Scintillation thermal plasma analysis package or SSIES (Rich & Hairston, 1994) measured the cross-track ionospheric convection flow at 1 s cadence (approx. 7 km spatial resolution). The Special Sensor Ultraviolet Spectrographic Imager or Special Sensor Ultraviolet Spectrographic Instrument (SSUSI) experiment (Paxton et al., 1992), measured auroral luminosity in a swath either side of the orbit in the Lyman-Birge-Hopfield short (LBHs) band, 140–150 nm (see Paxton and Zhang (2016); Paxton et al. (2017, 2021) and the references cited therein for further description of the instrument and data products). The Special Sensor for Precipitating Particles version 4 or SSJ/4 instrument (Hardy, 1984) provided measurements of precipitating ions and electrons between 30 eV and 30 keV, in 19 logarithmically spaced energy steps, at a cadence of 1 s.

The Super Dual Auroral Radar Network (SuperDARN) (Chisham et al., 2007) provided measurements of ionospheric flows in the NH. Observations from multiple radars are combined using a fitting procedure known as "map-potential" to deduce the global pattern of electrostatic potential (Ruohoniemi & Baker, 1998); as the radars do not cover all local times, a statistical model is used to fill in the gaps. We also present observations of the NH and SH field-aligned currents (FACs) derived from magnetometer measurements onboard the satellites of the Iridium telecommunications constellation processed using the Active Magnetosphere and Planetary Electrodynamics Response Experiment (AMPERE) technique (Anderson et al., 2000; Coxon et al., 2018; Waters et al., 2001). These observations cover all local times, but a spherical harmonic fit is used to interpolate between the spacecraft orbits.

The interval of interest is 17–19 March 2013, inclusive, encompassing the St. Patrick's Day storm of 2013. The IMF conditions, derived from the OMNI data set (King & Papitashvili, 2005), which drove this storm are shown in panel (g) of Figure 2. A step in solar wind ram pressure arrived at Earth shortly before 06 UT on 17 March (not shown), accompanied by an enhancement in the IMF magnitude. The GSM B_Y and B_Z components of the IMF fluctuated until 15 UT; from 15 UT B_Z was consistently negative until approximately 00 UT on 18 March, producing the main phase of the storm. For the majority of the next 50 hr, B_Z was positive and B_Y near zero, such that the clock angle, $\theta = \mathrm{atan2}(B_Y, B_Z)$, shown in panel (h), was close to 0°. Periods of small clock angle are highlighted by vertical lines, being 01 to 12 UT and 15 to 20 UT on 18 March, and 04 to 15 UT on 19 March; we will refer to these as intervals I, II, and III, respectively.

Panels (a)–(d) show "keograms" of auroral observations from the SSUSI instruments on DMSP F16 and F17 in the northern and southern hemispheres. These show the auroral emission in the LBHs band along the dawn-dusk meridian with a latitudinal resolution of 1° and a cadence of approximately 110 min (the orbital period of the spacecraft). Gray regions show missing data: either missing images, or portions of the dawn-dusk meridian that were not sampled (predominantly in the southern hemisphere). Panels (e) and (f) show corresponding keograms of FAC magnitude (red and blue for upwards and downwards FACs, respectively) from AMPERE, with a latitudinal resolution of 1° and a cadence of 10 min.

Prior to interval I, pairs of upwards/downwards FACs seen at dawn and dusk are the region 1 and region 2 (R1/R2) currents first identified by Iijima and Potemra (1976). A good correspondence between the location of the FACs and auroras is seen. Field-aligned currents and auroras are mainly located between colatitudes of 16 and 20° before the arrival of the shock, and between 20 and 35° during the storm main phase. The enlarged polar cap indicates that the open flux content of the magnetosphere, F_{PC}, was enhanced during the period of strong driving. From the start of interval I until 19 UT on 19 March the auroras and FACs contracted polewards, being mainly located polewards of 18° colatitude, and were weak. The FACs were no longer R1/R2 currents (which are associated with convection during southward IMF (Milan, 2013; Milan et al., 2017), but as will be discussed below were produced by dayside processes during NBZ. During intervals I and III, especially as observed by DMSP F16, the auroras extended virtually all the way to the poles such that the polar cap almost disappeared, and indeed later we will argue that the magnetosphere was probably nearly closed at these times. At the end of the interval, after 20 UT on 19 March, the IMF rotated southwards, the R1/R2 FACs reappeared and the auroras and FACs progressively expanded to lower latitudes, with an open polar cap.

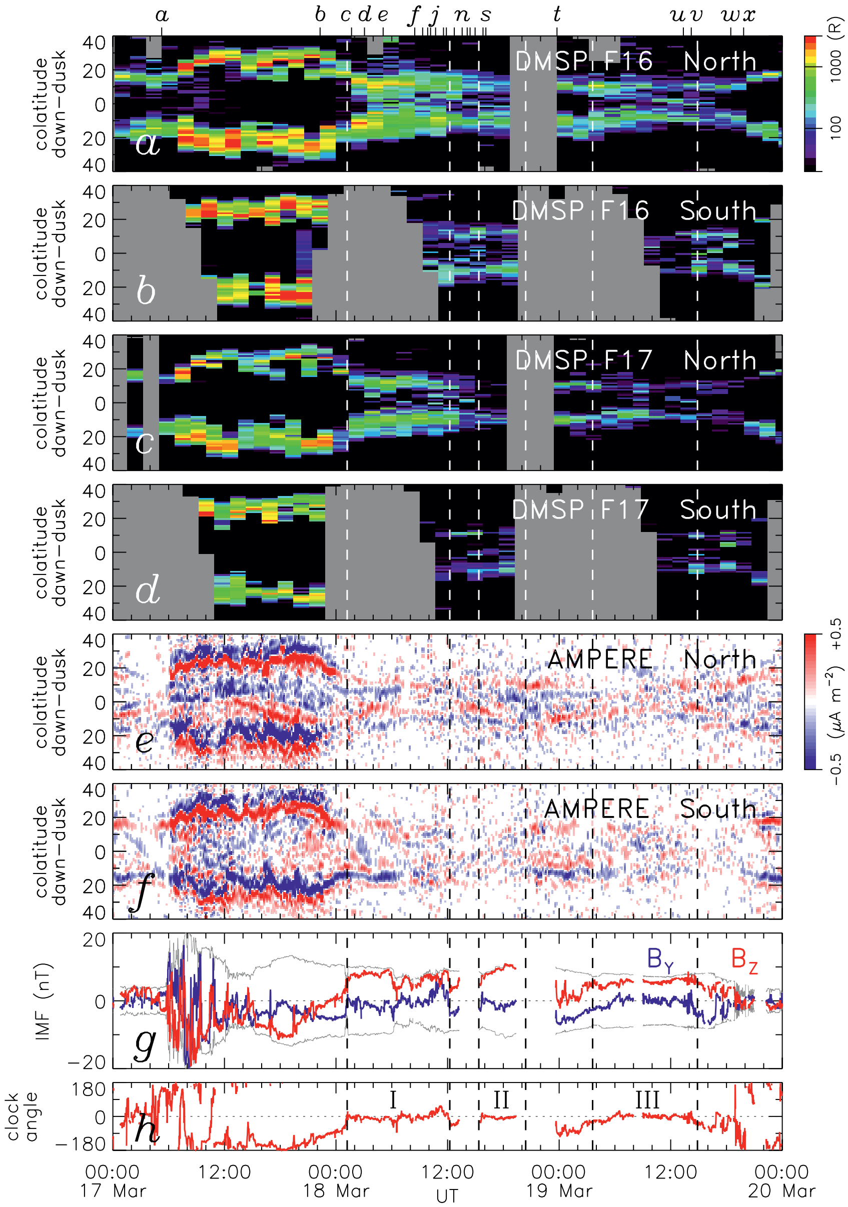

Figure 2. Observations of auroras, field-aligned currents, and interplanetary magnetic field for three days, 17–19 March 2013. (a–d) Auroral observations along the dawn-dusk meridian in the northern and southern hemispheres from the Special Sensor Ultraviolet Spectrographic Instrument instruments on Defense Meteorological Satellite Program F16 and F17. (e and f) Active Magnetosphere and Planetary Electrodynamics Response Experiment observations of field-aligned current density along the dawn-dusk meridian in the northern and southern hemispheres. Red and blue shading indicate upwards and downwards field-aligned currents, respectively. (g) Interplanetary magnetic field (IMF) B_Y (blue) and B_Z (red) components, and total IMF field strength (gray). (h) IMF clock angle. Three periods of near-zero clock angle, labeled I, II, and III, are indicated by vertical dashed lines. Tick marks at the top correspond to panels in Figure 3.

Tick marks and letters at the top of Figure 2 refer to panels of Figure 3, which show the auroras observed in the LBHs band by the SSUSI instrument during passes of DMSP F16, F17, and F18 over the northern and southern hemispheres. Noon is to the top and dawn to the right of each panel. Gray circles show lines of magnetic latitude in steps of 10°; note that all panels are on the same grid, expect panel (b) which extends to lower latitudes as this occurs during the main phase of the storm. Superimposed on each panel is the cross-track component of the ionospheric flow as measured by the ion driftmeter (IDM), with a scale shown in panel (a). The dial in each panel shows the concurrent IMF vector in the $B_Y - B_Z$ plane, the radius of the circle representing a magnitude of 10 nT.

10.1029/2021JA030089

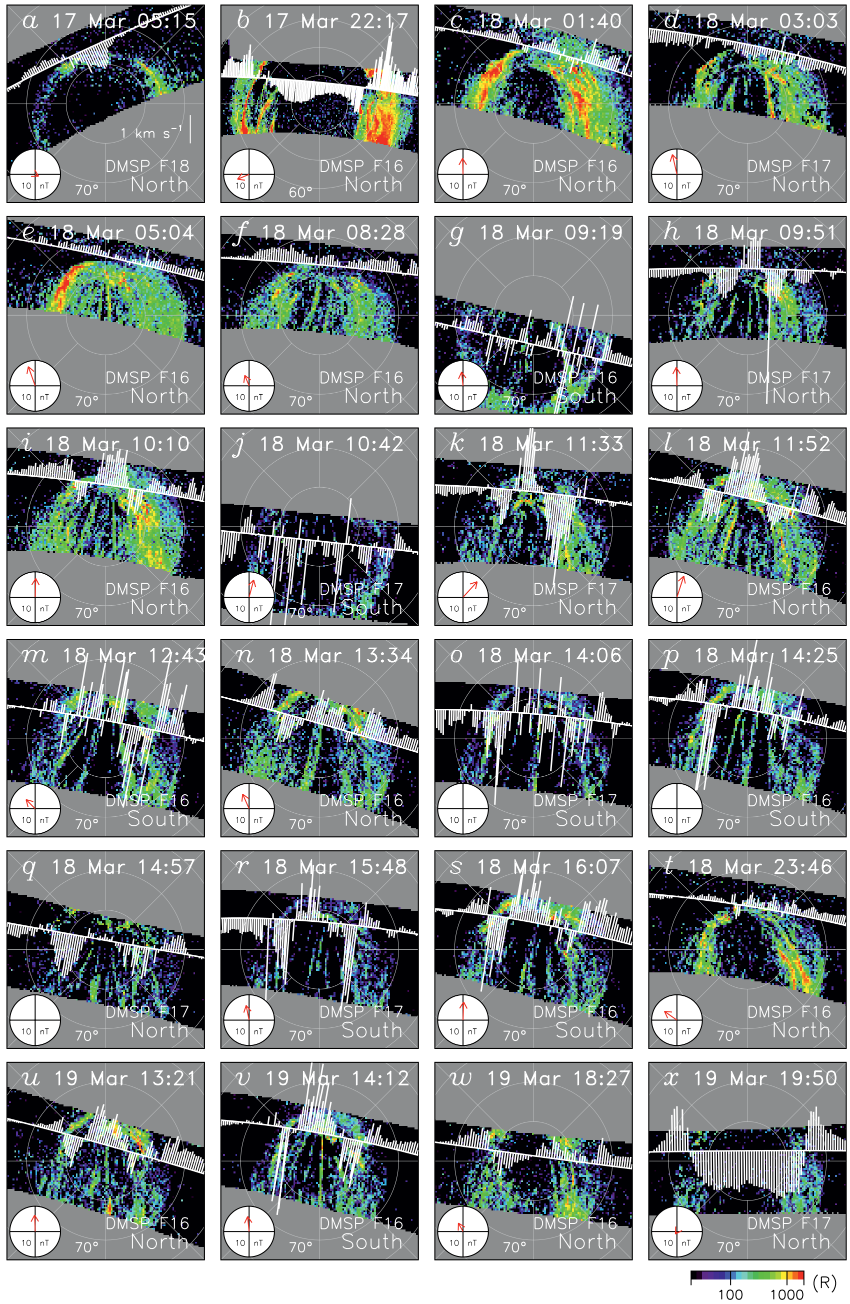

Figure 3. Observations of the auroral emission made by the Special Sensor Ultraviolet Spectrographic Instrument instruments onboard Defense Meteorological Satellite Program (DMSP) F16, F17, and F18 on 17–19 March 2013 on a geomagnetic latitude and local time grid, with noon toward the top. Circles indicate latitudes of 60, 70, and 80°; note all panels are on the same scale, except (b) which extends to lower latitudes. Superimposed on each panel are cross-track ionospheric flow vectors from the Ion Driftmeter instrument on DMSP, with the scale indicated in panel (a). The dial plots show the IMF B_Y and B_Z components (when available), with the circumference of the circle representing 10 nT. For reference, 1 kR in the Lyman-Birge-Hopfield short band corresponds approximately to an International Brightness Coefficient class 1 visible aurora (Chamberlain, 1961), or 1 erg cm^{-2} s^{-1} (1 J m^{-2} s^{-1}).

Panel (a) is from the period prior to the shock arrival and shows a typical auroral oval configuration with an empty polar cap; the spacecraft track is too far toward the dayside to unambiguously identify the ionospheric flow pattern, but the observed flows are consistent with a standard twin-cell convection pattern. Panel (b) is from the main phase of the storm, and shows bright auroras expanded to low latitudes, an enlarged polar cap, and strong twin-cell convection.

Panels (c)–(e) are from the beginning of interval I, when the IMF has clock angles $|\theta| < 20°$ and DLR might be expected to occur. Unfortunately, the DMSP orbit is not able to confirm the convection pattern during this period (though this will be discussed further below). However, the auroral evolution at this time is consistent with the DLR scenario described by Milan, Carter, Bower, et al. (2020): in panel (c) the auroras have contracted to high latitudes, but a clear polar cap is still observed; in panel (d) cusp-aligned arcs appear poleward of the dawn and dusk sectors of the auroral oval; and in panel (e) the polar regions are filled with auroras, with the appearance of multiple cusp-aligned arcs. Milan, Carter, Bower, et al. (2020) interpreted similar observations as the closure of open flux by DLR, producing sunward ionospheric flows across the noon sector polar cap boundary, and the distribution of this newly closed flux to the high-latitude dawn and dusk sectors by antisunwards flows; however, in this example that process has continued and the whole polar regions have filled with auroras. Prior to DLR the open field lines are evacuated of plasma, so the polar cap is largely devoid of auroras; however, the newly closed flux is expected to be laden with captured solar wind plasma, which could give rise to the auroral emission seen at high latitudes.

Most other panels in Figure 3 show that the polar regions were filled with cusp-aligned arcs for the majority of the time until the end of interval III. Here we will describe just a few particular examples and return to others in the Discussion. From panels (h) to (v) the orbits of the spacecraft allow the dayside convection pattern to be measured, and confirm the flows expected for DLR, that is, sunward near noon and antisunward flows into the high-latitude dawn and dusk sectors, and sometimes sunward flows at latitudes below the main auroral emission.

Panels (t) and (w) show periods when the IMF has rotated to $|\theta| \sim 45°$, when DLR is no longer expected to occur but single lobe reconnection (SLR) will open flux (see Discussion) and produce lobe stirring. In both cases the polar regions become devoid of auroras suggesting an open polar cap. In the case of panel (w), the ionospheric flows confirm the expected convection pattern for SLR. Between these times, panels (u) and (v) show that when the IMF returns to low clock angles the flow pattern becomes consistent with DLR again, and the polar cap refills with auroras in both the northern and southern hemispheres.

In panel (x) the IMF has rotated to become southwards, the convection pattern becomes twin-celled and the polar cap is open, consistent with the observations at this time in Figure 2.

Figure 4 shows AMPERE-derived FAC density, in both the northern and southern hemispheres, at four selected times. At each time, especially in the northern hemisphere, the FACs are consistent with DLR and the vorticity of the associated convection pattern (often referred to as northward IMF B_Z or NBZ FACs (Iijima et al., 1984)). Reverse, lobe cells are expected to be accompanied by a pair of up/down FACs straddling noon at latitudes near or above 80°, with reversed-polarity FACs at lower latitudes, as discussed by Milan, Carter, Bower, et al. (2020). Such a pattern is observed in all panels (except the SH in panel (a)), but the strength of the FACs is greatest in the northern hemisphere. The strength of NBZ FACs is anticipated to be controlled by the conductance of the ionosphere (Fujii & Iijima, 1987; Milan et al., 2017), though it is not expected that there will be much hemispherical asymmetry in the conductance in these near-equinox observations. The location of the solar terminator (green) in each hemisphere suggests that the conductance will be somewhat higher in the northern hemisphere, except in panel (a).

Panel (b) indicates that the ionospheric flows measured by IDM are consistent with the pattern expected for lobe reconnection with near-zero IMF B_Y. This could be associated with SLR occurring in just the northern hemisphere, but as similar flow patterns are seen also in the southern hemisphere throughout the interval, it is likely that DLR is ongoing. This is supported by the hypothesis that DLR results in the production of closed magnetic flux at high latitudes (Milan, Carter, & Hubert, 2020), which we argue below. Concurrent SuperDARN measurements (right-most panel) show reverse twin-cell convection associated with the NBZ FACs and weak nightside flows which are generally antisunwards along the midnight meridian with return flows at dawn and dusk, consistent with average flow patterns for purely northwards IMF (e.g., Thomas & Shepherd, 2018). Panels (c) and (d) (corresponding to panels (u) and (v) in Figure 3) show that DLR flows of similar speeds are observed in both the NH and SH, despite the difference in FAC magnitudes. The polar regions are filled with auroral forms in both NH and SH. That is, the flows and auroras resulting from DLR are highly symmetrical in the two hemispheres.

Panel (a) occurs at the start of interval I (and corresponds to Figure 3c), during the period that the horse-collar formation of auroras is first developing. Although earlier we could not confirm that DLR flows were occurring at this time, due to the orbit of the DMSP spacecraft, here we see that the DLR FAC pattern is indeed present. The

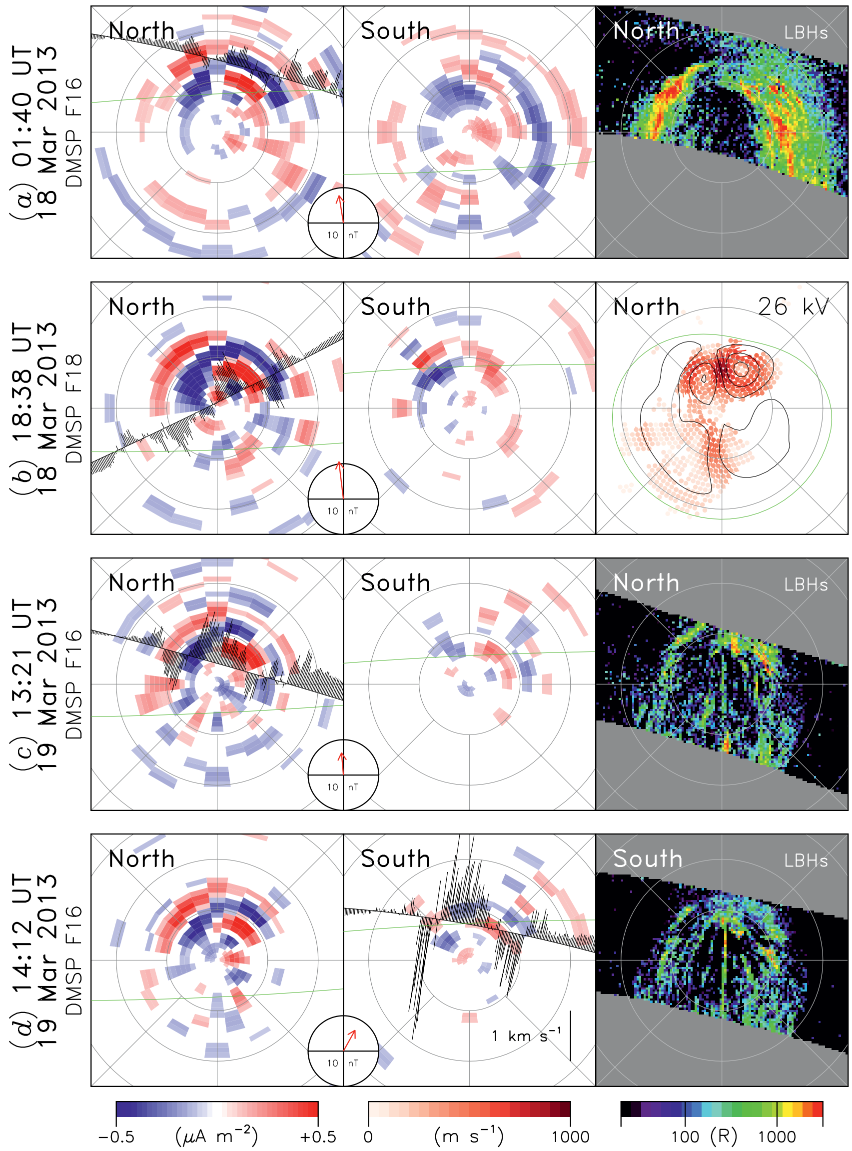

Figure 4. Left and middle panels show Active Magnetosphere and Planetary Electrodynamics Response Experiment observations of field-aligned current density in the northern and southern hemispheres at times of selected passes by Defense Meteorological Satellite Program. The data are presented on a geomagnetic latitude and local time grid, with noon at the top and circles representing latitudes of 60, 70, and 80°, with the solar terminator indicated in green. Cross-track ionospheric flow vectors from the Ion Driftmeter are superimposed on the hemisphere in which the pass occurred; the scale is indicated in panel (d). The dial plots show the interplanetary magnetic field B_Y and B_Z components. Right panels show the auroral emission measured by the Special Sensor Ultraviolet Spectrographic Instrument (panels a, c, and d) or the ionospheric flow pattern inferred from Super Dual Auroral Radar Network observations (panel b); in the latter, the green circle is the low latitude extent of the convection pattern. The location of radar observations and the convection speed are indicated by shading; contours of electrostatic potential are indicated in steps of 6 kV.

DLR FACs in panel (a) are located at slightly lower latitudes than those in panels (c) and (d), as are the auroral emissions as a whole. This suggests that the presence of an open polar cap affects the location of the auroras and associated FAC patterns, by moving them to lower latitudes.

We now turn to an investigation of the particle signatures observed during four representative orbits of DMSP: Figure 5 in which the satellite track passes the sunward-most edge of the auroral emission, Figure 6 in which the spacecraft crosses the NBZ FACs, Figure 7 in which the track is antisunwards of the NBZ FACs, and Figure 8 in which the nightside is observed. All are presented in the same format. The AMPERE FACs in both NH and SH

10.1029/2021JA030089

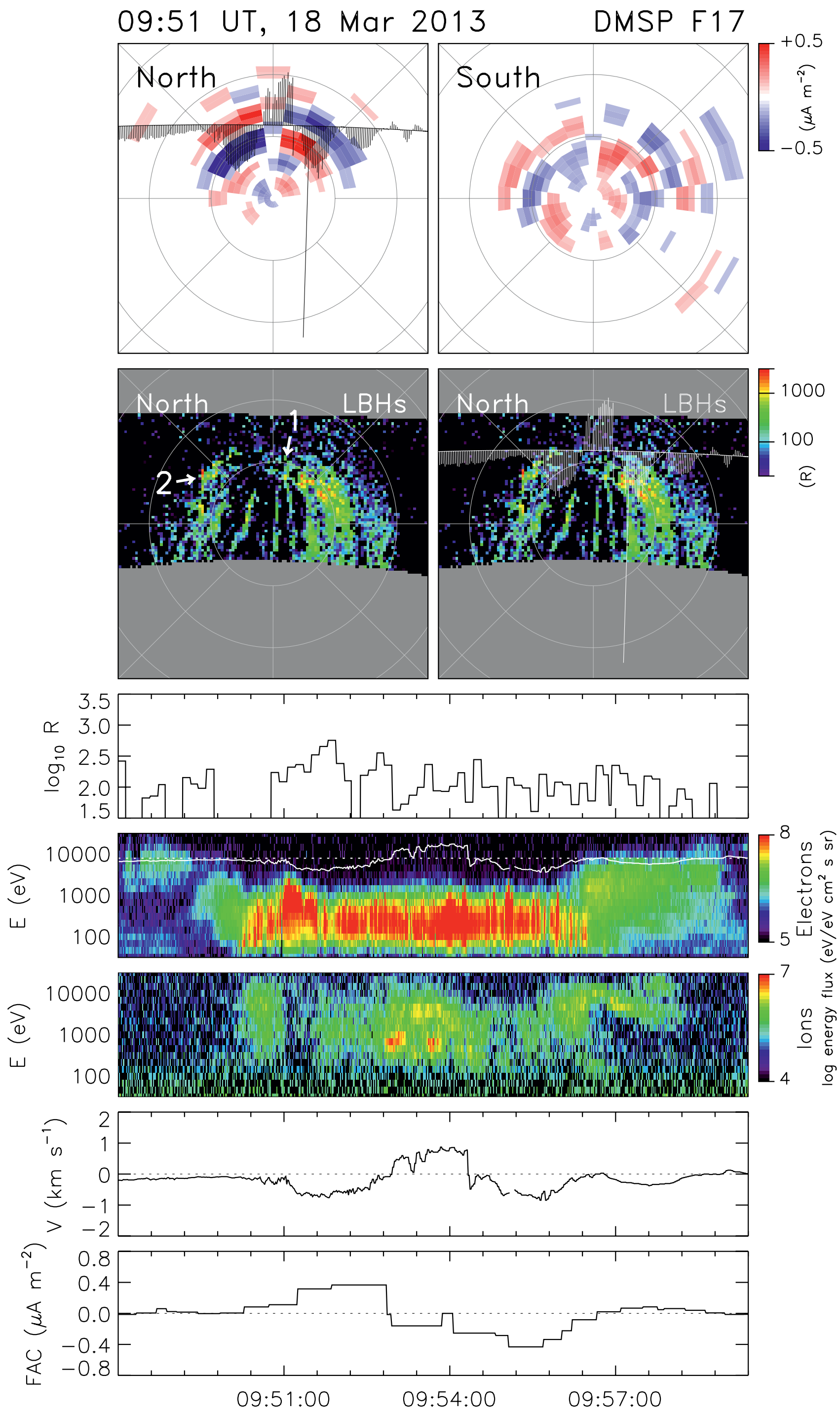

Figure 5. Observations from a pass of the northern hemisphere by Defense Meteorological Satellite Program F17 around 09:51 UT on 18 March 2013. Top panels show Active Magnetosphere and Planetary Electrodynamics Response Experiment (AMPERE) observations of field-aligned current density in the northern and southern hemispheres at the time of the pass (averaged over the duration of the pass), presented on a geomagnetic latitude and local time grid with noon at the top. Circles indicate geomagnetic latitudes of 60, 70, and 80°. Ionospheric flow vectors from the Ion Driftmeter (IDM) are superimposed on the hemisphere in which the pass occurred. Below this, on the same grid, and auroral observations from the Special Sensor Ultraviolet Spectrographic Instrument (SSUSI), presented twice, once with and once without the flow vectors superimposed. Arrows indicate (1) the high-latitude dayside aurora and (2) an auroral blob associated with clockwise vorticity of the convection pattern (see text for details). The five panels below show parameters along the spacecraft track, over the duration of the pass. These are: auroral emission intensity from SSUSI, precipitating electron and ion spectrograms from the SSJ/4 instrument, the speed of the cross-track flow (positive sunwards) from IDM (also shown on the electron spectrogram), and the field-aligned current density from AMPERE.

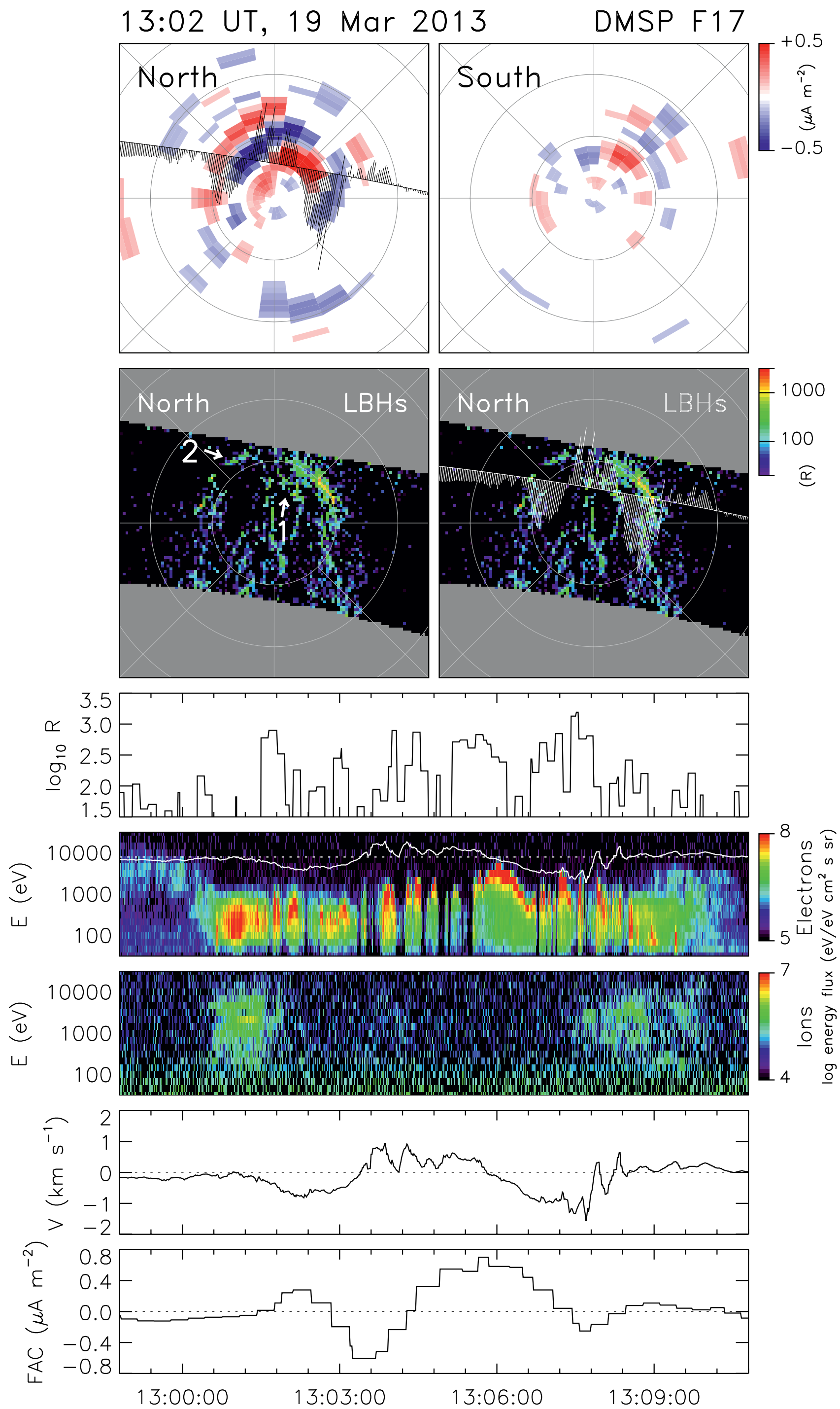

Figure 6. Similar to Figure 5, for the northern hemisphere pass of Defense Meteorological Satellite Program F17 around 13:02 UT on 19 March 2013.

are shown at the top, with the IDM measurements superimposed on the hemisphere in which the pass occurred. In the next row, the SSUSI LBHs observations are shown twice, with the IDM measurements superimposed in the right-hand panel. The panels below these show measurements along the DMSP track as a function of time; in the case of SH passes the time axis is reversed so that in all cases the observations are presented with dusk at the left and dawn at the right. These panels show the SSUSI radiance intensity under the spacecraft, spectrograms of the precipitating electrons and ions from SSJ/4, the cross-track flow speed ($V_{\perp}$, positive sunwards) from IDM

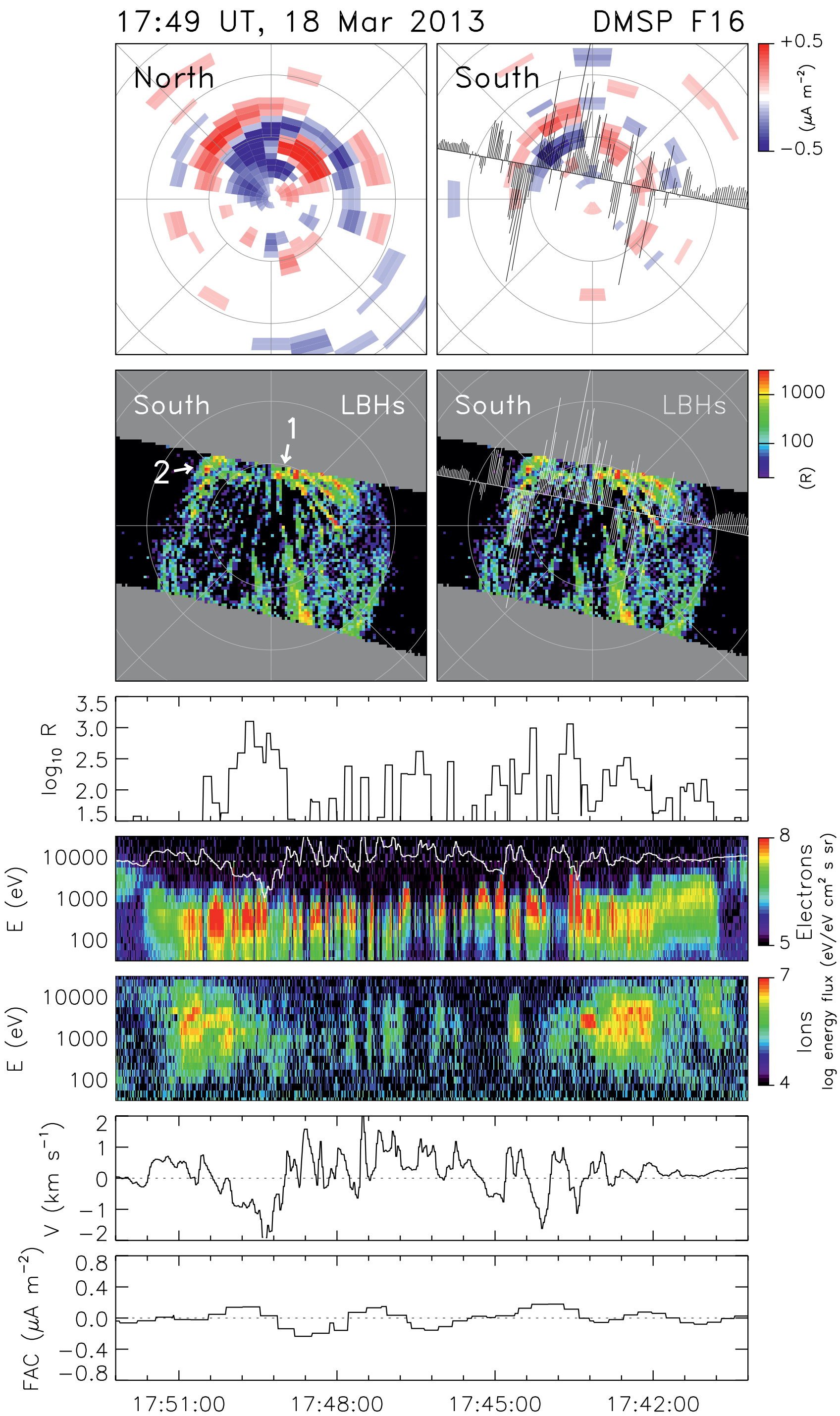

Figure 7. Similar to Figure 5, for the southern hemisphere pass of Defense Meteorological Satellite Program F16 around 17:49 UT on 18 March 2013. Note that for this pass of the southern hemisphere, the time axis has been reversed so that left and right correspond to dusk and dawn.

(also superimposed on the electron spectrogram), and the FAC magnitude (positive upwards) along the spacecraft track, derived from the AMPERE observations.

In Figure 5 (corresponding to Figure 3h), DMSP F17 passes at the sunward edge of the auroras. The DLR-driven flow pattern is very clear in the IDM measurements, with little small-scale structure superimposed on the the

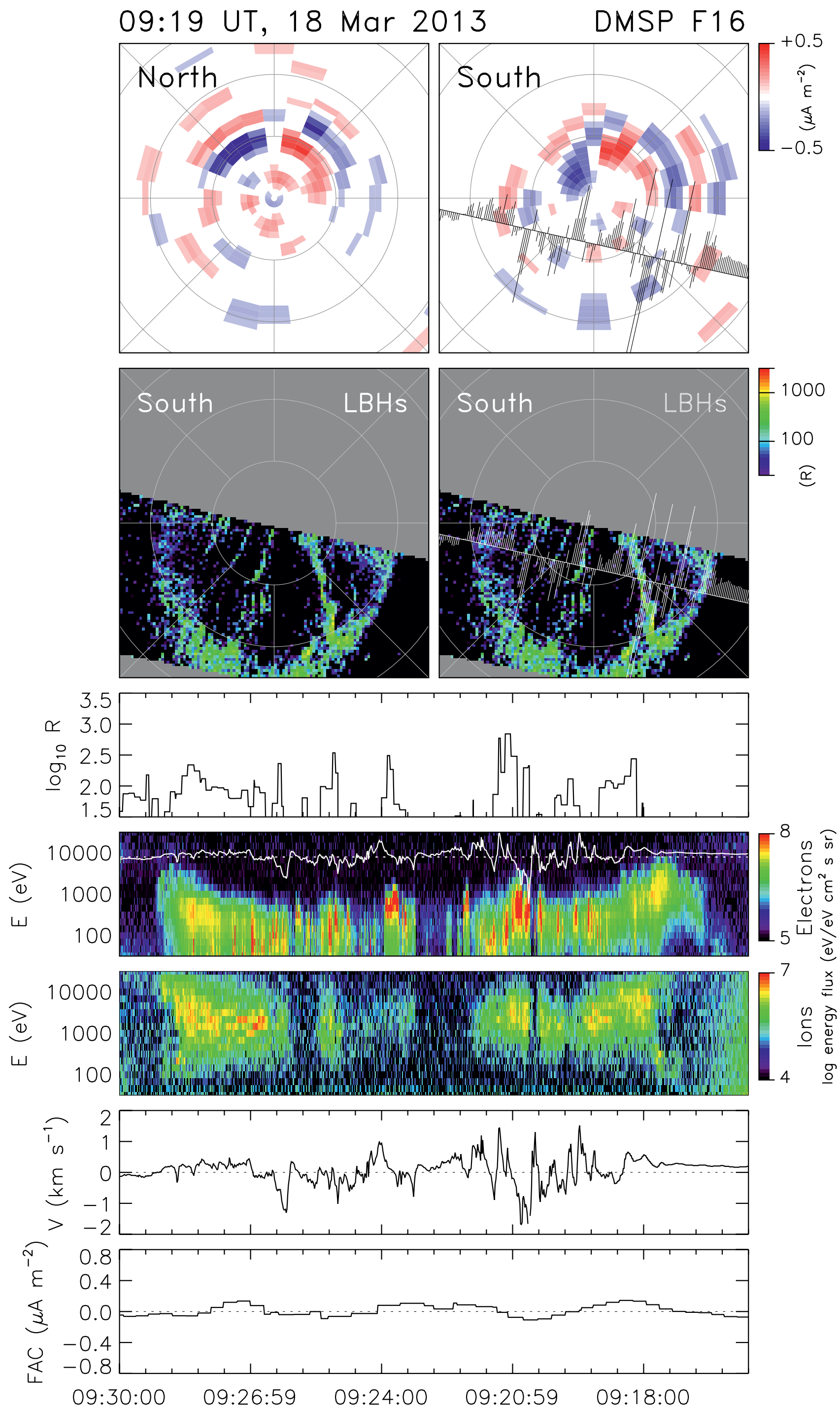

Figure 8. Similar to Figure 5, for the southern hemisphere pass of Defense Meteorological Satellite Program F16 around 09:19 UT on 18 March 2013. Note that for this pass of the southern hemisphere, the time axis has been reversed so that left and right correspond to dusk and dawn.

antisunwards/sunwards/antisunwards convection. At lower latitudes, hot electrons (up to and exceeding 10 keV) are observed, the signature of trapped plasma on closed field lines produced during the normal Dungey cycle. Polewards of this are intense low energy (up to 1–2 keV) electrons and ions with a broad range of energies; the highest fluxes of ions are observed in the region of sunward flow. We interpret these ions and electrons as magnetosheath plasma precipitating downstream of the lobe reconnection site (i.e., sunwards of the ionospheric projection of the x-line). If we could observe the particle characteristics along the noon meridian we would expect a reverse dispersed ion signature within the sunward convection throat (Woch & Lundin, 1992).

We note an increase in electron energies observed at 09:51 UT, at the duskward edge of the convection pattern. In this region there is a negative gradient in $V_\perp$, which implies converging electric field and hence upward FAC, consistent with the AMPERE measurements. We interpret this as a region in which electrons are accelerated downwards to carry the required FAC, producing a region of auroral emission near the 15 MLT meridian (arrow labeled 2). Examination of the panels in Figure 3 reveals that this blob of auroral emission is a consistent feature of the observations, though does change in location and extent from image to image.

In Figure 6 (corresponding to a time close to Figure 3u), DMSP F17 passes further toward the pole and crosses the main region of NBZ FACs, with the down/up FAC pattern clearly observed in the bottom panel. The DLR flow pattern is again clear, but now there is more small-scale structure superimposed on the convection, with ± 500 m s^{-1} flow variations seen around 13:04 and 13:08 UT. As F17 traverses from sunward to antisunward flow at 13:06 UT, a clear, broad inverted-V signature is seen in the electrons, co-located with a region of pre-noon auroral emission (arrow labeled 1). We note that no ions are associated with the inverted-V structure, consistent with similar observations by Cai et al. (2021). Narrower inverted-V structures are seen to be associated with negative gradients in $V_\perp$ where the small-scale but large-amplitude fluctuations are seen, both within the sunward flow region and the dawnside antisunward flow region.

The pre-noon auroral blob (a) associated with upward FAC identified in Figure 5 is the high-latitude dayside aurora (HiLDA) discussed in case studies by Frey (2007) and Cai et al. (2021) and statistically by Carter et al. (2018). HiLDAs are produced by the upward FAC associated with the clockwise vorticity of the NBZ reverse convection pattern, as can be seen by comparing the velocity panel in Figure 6 with the electron precipitation panel at the time span where the large inverted-V structure appears (13:05:30–13:07:00). Re-examination of the observations presented by Carter et al. (2018) reveals that on average a post-noon auroral blob is also observed co-located with the region one polarity FAC, similar to the post-noon auroral blob (b) identified in Figure 5. Both are produced by precipitation associated with upward FAC due to the vorticity of the convection pattern, and the same morphology is observed in both NH and SH.

The pass of F16 in Figure 7 is similar to that in Figure 5, though crosses the noon meridian slightly antisunwards of the HiLDA. The figure shows multiple cusp-aligned arcs, and associated flow-shears and inverted-V structures, pointing into the cusp region and even merging with the HiLDA, that is, reaching into the center of the pre-noon DLR flow vortex. This pass also shows that the cusp-aligned arcs sunwards and antisunwards of the dawn-dusk meridian do not necessarily connect with each other, though this is discussed further below. Patches of ion precipitation are seen across the polar regions, suggesting that significant regions of closed flux exist. We note that unlike the HiLDA FAC, in which inverted-V electron precipitation is seen, but no ions, both ions and electrons can co-exist where the cusp-aligned arcs FACs are observed.

In Figure 8, F16 passes antisunwards of the pole, crossing several prominent cusp-aligned arcs. The flows are highly structured, with multiple narrow sunward/antisunward flow shears with amplitudes in excess of ± 1 km s^{-1}. Negative gradients in $V_\perp$ are associated with inverted-V signatures and colocated cusp-aligned arcs. These signatures are highly reminiscent of the observations reported by Zhang et al. (2020). Ion precipitation is observed across most of the polar traversal, suggesting that the magnetic flux is closed; a relatively narrow region is devoid of ions between the two main cusp-aligned arcs, which might be interpreted as the poleward edges of the dawn and dusk regions of the HCA, indicating that the central region of flux could be open. Despite F16 crossing several arcs, no clear FAC signatures are seen by AMPERE along the track, probably as a consequence of the relatively coarse spatial resolution of the observations.

Figure 9 (corresponding to Figure 3m) shows superimposed observations from F16 and F18 as they traverse the SH polar regions at almost exactly the same time, with F18 and F16 sunward and antisunward of the pole. Once again the flows are highly structured, with flow shears being colocated with inverted-V electron precipitation and cusp-aligned auroral arcs. F18 observes mostly sunward flows near the noon meridian, but with large perturbations superimposed. There is consistency between the flows observed in the dawn sector where the spacecraft pass close to each other, but it is difficult to discern the how the patterns fit together at dusk. It is probable that the nature of the flows is ordered by the pattern of cusp-aligned arcs—indeed, a flow shear is seen at each

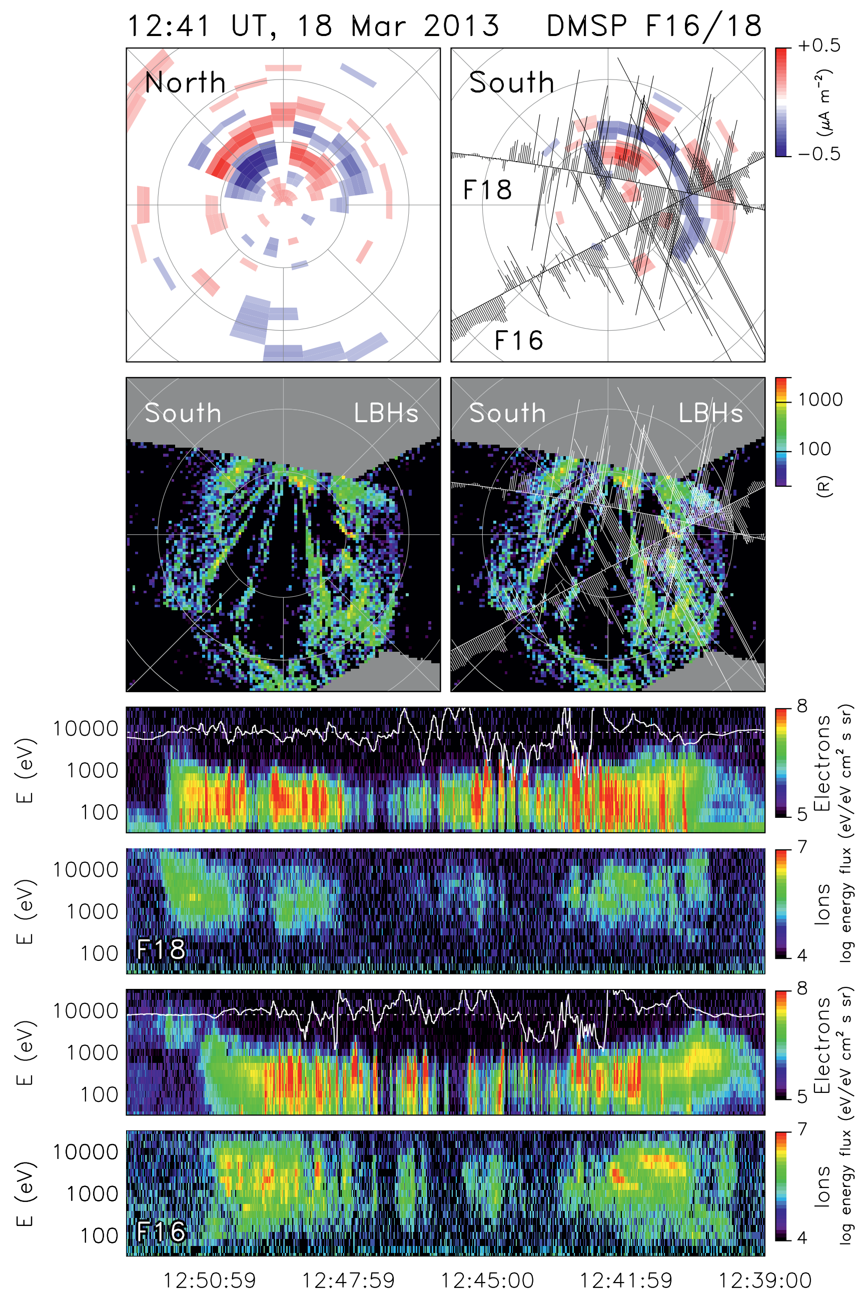

Figure 9. Observations from near-simultaneous passes of the southern hemisphere by Defense Meteorological Satellite Program F16 and F18 around 14:41 UT on 18 March 2013. The auroral observations from the Special Sensor Ultraviolet Spectrographic Instrument on the two spacecraft have been superimposed. At the bottom, electron and ion spectrograms from SSJ/4 on the two spacecraft are shown, with ionospheric flows from the Ion Driftmeter superimposed.

arc-crossing—but the convection is clearly complicated and presumably time-variable. Ion precipitation present along both spacecraft tracks, especially on the nightside, suggest that much of the polar magnetic flux is closed.

In Figure 10 we examine the SuperDARN observations in more detail. Four radars of the network—Rankin Inlet, Inuvik, Hankasalmi, and Pykvibaer—contribute most to the measurements, and the line-of-sight velocity derived from the backscatter observed by each are shown in the left-hand panels (separated into two panels to avoid overlap), at five selected times. When combined using the standard SuperDARN "map-potential" fitting procedure (Ruohoniemi & Baker, 1998), these measurements give rise to the convection pattern presented in Figure 4b. The central beam of the Rankin Inlet radar looks almost directly into the convection throat at noon, observing sunward

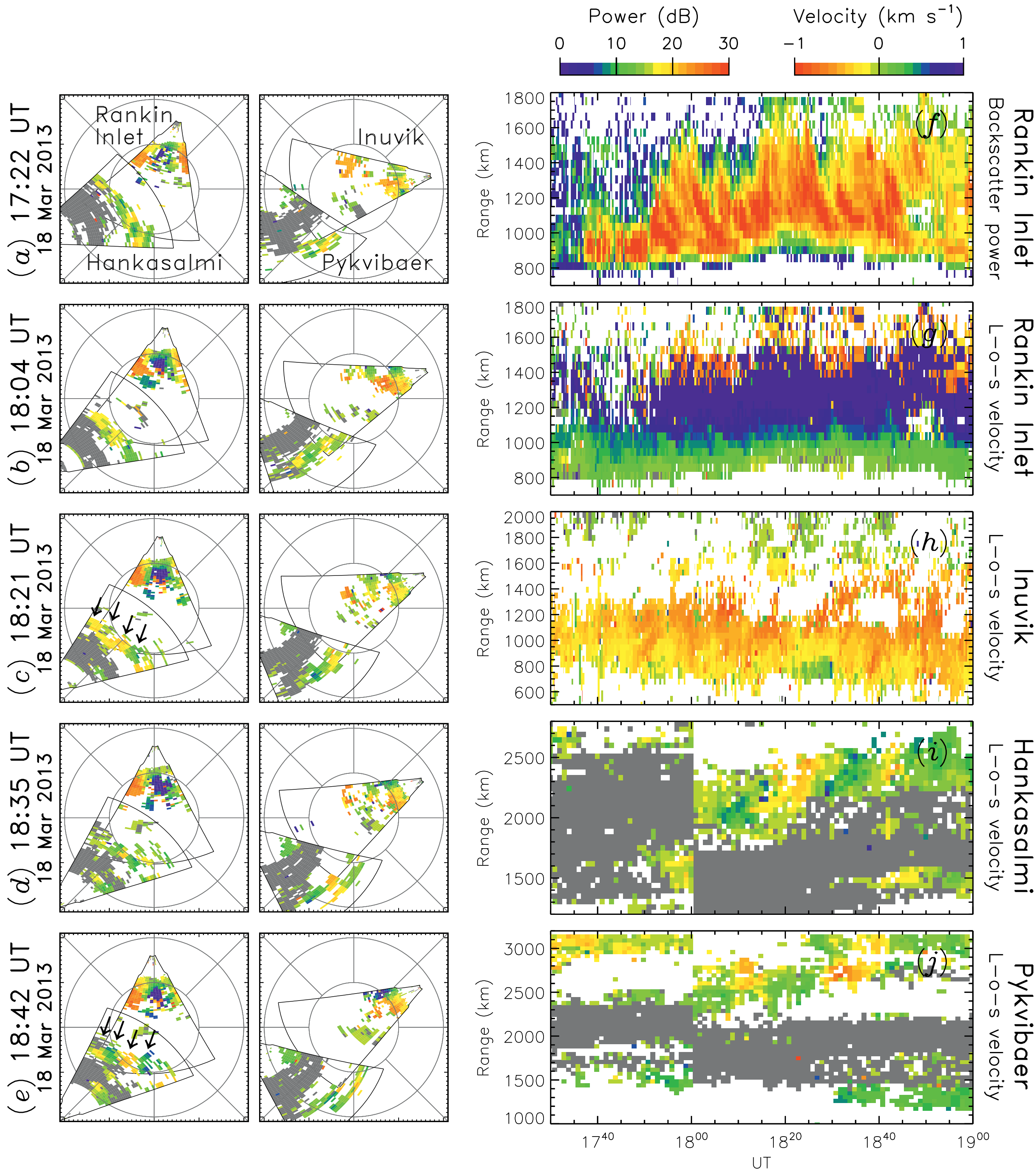

Figure 10. Super Dual Auroral Radar Network observations of northern hemisphere ionospheric flows between 17 and 19 UT on 18 March 2013, from the Rankin Inlet, Hankasalmi, Inuvik, and Pykkvibaer radars. On the left, measurements of line-of-sight flow speed (blue toward and red away from the radars) are presented on a geomagnetic latitude and local time grid, with noon at the top (in two separate panels to avoid overlap); concentric circles represent latitudes of 70° and 80°. To the right, range-time-parameter plots are presented of backscatter power from the Rankin Inlet radar, and line-of-sight flow speed for each of the four radars. In each case observations are shown from beam six of the radars, as these are roughly central beams, and because the Rankin Inlet and Inuvik radars were scanning this beam at a higher than usual temporal cadence (roughly 20 s as opposed to 2 min). Gray indicates echoes that have been classed as ground backscatter. Note that a change of operating frequency occurred at 18 UT at the Hankasalmi and Pykkvibaer radars.

flows up to 1.5 km s^{-1} (toward the radar, blue); to either side antisunward flows (away, red) are seen, consistent with the DLR convection pattern. This pattern of flows is observed by Rankin Inlet over the whole 1.5 hr period shown, confirmed by the range-time-velocity panel (g). Flows are strongest and weakest at the farthest and nearest ranges, consistent with the rotation of the flow within the DLR throat region from sunwards to dawnwards and duskwards as latitude decreases. Panel (f) shows the corresponding range-time-power measurements. Regions of higher backscatter power are seen to quasi-periodically (3–6 min) propagate toward the radar; the curved nature of the striations suggests deceleration along the line-of-sight, consistent with the gradient in the velocity, and we suggest that regions of enhanced backscatter power are entrained within the convection as it circulates within the DLR pattern. Although not obvious with the color scale employed, these power enhancements are accompanied by fluctuations in the convection speed with an amplitude of several 100s m s^{-1} superimposed on the background ~1 km s^{-1} flow. The nature of these sunward-propagating power/velocity fluctuations is similar to poleward-moving radar auroral forms (PMRAFs) observed in the dayside polar cap during southward IMF, which are the counterpart of poleward-moving auroral forms produced by flux transfer events (FTEs), that is quasi-periodic bursts of low latitude reconnection (e.g., Milan et al., 2000a; Pinnock et al., 1995; Provan et al., 1998; Wild et al., 2001). The observations of Figure 7 come from this interval. It is interesting to speculate if the time-variable flows observed by SuperDARN are associated with the cusp-aligned arcs observed to be reaching into the cusp region.

Flows on the nightside are monitored by the Hankasalmi and Pykvibaer radars. The fitted convection pattern, Figure 4b, shows relative weak and smooth flows on the nightside, in contradiction to the highly structured flows observed by DMSP IDM (Figures 7 and 8). However, both nightside radars do observe toward/away line-of-sight velocity enhancements with speeds of several 100s m s^{-1} (highlighted by arrows) that come and go and move about. The corresponding range-time-velocity panels, (i) and (j), show variations in the flow with periods close to 20 min. We conclude that structured flows are indeed observed by SuperDARN during this interval, but that the spatial resolution of the map-potential fitting procedure is too coarse to properly characterize this. The DMSP observations also imply that there are many small-scale FACs, accompanied in the case of upwards FACs by cusp-aligned arcs, but these are not resolved by the spatial resolution of the AMPERE technique.

3. Discussion

Following the main phase of the geomagnetic storm of St. Patrick's Day 2013, the IMF had near-zero clock angle for long periods over the next two days. Observations of auroral emissions, ionospheric flows, and field-aligned currents suggest that during these northward IMF periods the magnetosphere underwent DLR, closing open magnetic flux (Cowley, 1981; Dungey, 1963). This lead first to a horse-collar auroral configuration (e.g., Elphinstone et al., 1993; Hones Jr et al., 1989; Milan, Carter, Bower, et al., 2020; Murphree et al., 1982) before the whole polar regions became full of cusp-aligned auroral arcs. We interpret this as partial and then almost full closure of the magnetosphere. We anticipate that the poleward edge of the HCAs at dawn and dusk map to the magnetopause of the dawn and dusk flanks of the magnetosphere, encompassing the newly closed flux that is appended to the magnetosphere by DLR. If this process continued to full closure of the magnetosphere, we would expect that the dawn and dusk magnetopause would map to a line running along the noon-midnight meridian, and there are times when such an auroral arc is observed, for instance Figure 4 panels (c) and (d). If the magnetosphere does close entirely, then DLR should drive reverse convection (Siscoe et al., 2011; Song et al., 1999), and in general the observed flows are consistent with this. In addition, the observation of (presumably trapped) ion precipitation across most of the traversals of the polar regions by DMSP (Figures 7 and 8) suggest significant flux closure. On the other hand, as seen in Figure 2, when the clock angle deviates from near-zero, the polar cap re-expands.

Figure 1 summarizes the reconnection geometries available at the magnetopause for southward and northward IMF: (a) low latitude reconnection, (b) single lobe and (c) DLR in an open magnetosphere, and (d) single lobe and (e) DLR in a closed magnetosphere. Scenario (a) increases the open flux (the polar cap flux, F_{PC}) in the magnetosphere and drives the Dungey cycle, (b) neither increases nor decreases F_{PC} but produces lobe stirring, (c) reduces F_{PC} and causes reverse convection mainly confined to the dayside polar regions. Scenario (d) opens flux, increasing F_{PC}, while (e) does not open flux but induces reverse convection throughout the outer magnetosphere and polar regions, as modeled by Song et al. (1999) and Siscoe et al. (2011).

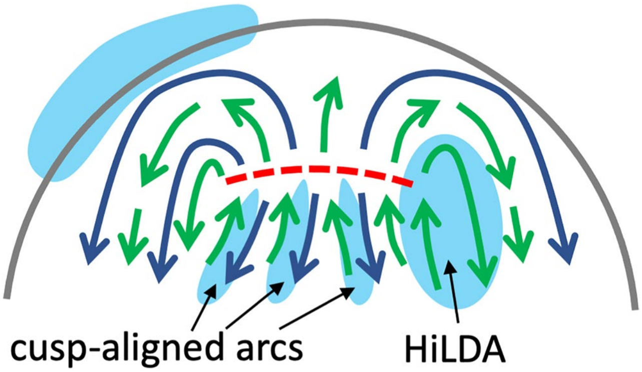

Figure 11. A schematic diagram of the ionospheric flows which could be driven by lobe reconnection in a magnetosphere that is nearly closed but has regions of open magnetic flux. The gray semicircle is the low latitude extent of the dayside convection pattern, with noon toward the top; the red dashed line is the ionospheric projection of the lobe reconnection x-line. Green and blue arrows show flow streamlines which might be driven for different reconnection geometries (see text for details). Blue shading indicates where vorticity in the flow will be associated with upwards field-aligned currents producing auroral emission, including the high-latitude dayside aurora and cusp-aligned arcs. The figure is not intended to be to scale; for instance, the width of the reconnection x-line is exaggerated for clarity.

For NBZ with near-zero IMF B_Y we expect first scenario (c) and then (e) to close the magnetosphere and then drive reverse convection within it. However, if B_Y becomes non-zero then (b) will halt the closure of the magnetosphere, and (d) will even reverse it. This is consistent with the disappearance of auroral emissions near the pole in Figure 3 panels (t) and (w). The southward turning of the IMF at the end of interval III, Figure 2, leads to low latitude reconnection which reopens the magnetosphere and drives Dungey cycle flows, as shown in Figure 3x. It is interesting to note that although the IMF magnitude is small (≈5 nT) and B_Z is only −1 nT at this time, the reopening of the magnetosphere is rapid and the strength of the flows is large. It appears that the magnetosphere "abhors a vacuum" and will reopen readily.

We anticipate that achieving full closure of the magnetosphere through DLR is difficult. As the magnetosphere approaches full closure, any IMF field line that reconnects in one hemisphere but not the other, as in scenario (d), will reopen flux. This failure to reconnect in both NH and SH could be caused by small variations in IMF B_Y, turbulence within the magnetosheath, or transient and/or episodic reconnection. It seems likely that during prolonged periods of near-zero clock angle, a complicated interleaving of regions of open and closed flux could be produced in the polar regions, with the magnetosphere nearly closed, but not entirely. Such bursty reconnection and the interleaving of open and closed flux could be related to the appearance of cusp-aligned arcs and fast flow channels, as discussed below.

That the magnetosphere is nearly closed explains why auroral emission can occur over the entire polar regions: the closed flux will contain plasma that can be accelerated to produce auroras; in contrast, the polar regions are usually devoid of auroras because the open lobes are evacuated. However, we have also shown that the auroral emission is not uniform, but comprises multiple cusp-aligned arcs. Although these arcs have been reported before, their origin is still uncertain. Zhang et al. (2020) showed that such arcs are associated with inverted-V precipitation signatures and filamentary field-aligned currents, associated with shears in the convection flow, just as presented in this paper. They suggested that these convection shears were propagated into the central magnetotail by Kelvin-Helmholtz Instability (KHI) waves on the magnetopause. In their scenario it is necessary for the magnetosphere to be nearly closed, such that closed flux from the central tail maps across the polar regions where the arcs are observed: DLR can provide this closure. Also, if the arcs are formed by the KHI and waves propagating from the magnetopause toward the central tail, we might expect to see a "phase motion" of the arcs in the ionosphere. This phase motion would be expected to emanate from the noon-midnight meridian (where the dawn and dusk flank magnetopause would map if the magnetosphere was closed) and move to lower latitudes both dawnwards and duskwards. Unfortunately, the cadence of the SSUSI images is too coarse to allow this behavior to be resolved.

Alternatively, we suggest that patchy and bursty lobe reconnection could also lead to flow channels with associated arcs, and that these flow channels would naturally focus in toward the cusp region, giving the appearance of "cusp-aligned arcs". The interleaving of open and closed flux described above will lead to different reconnection geometries (as exemplified in Figure 1) at different points along the x-line (See also the discussion in Fear et al. (2015) in the context of transpolar arcs.). The spatially and temporally structured ionospheric flows observed by the Rankin Inlet radar are indicative of bursty reconnection. A possible scenario is sketched in Figure 11. The gray semicircle represents the low latitude extent of the dayside convection pattern, and the red dashed line is the ionospheric projection of the lobe x-line. A complicated pattern of open and closed flux is envisaged across the polar regions. Portions of the x-line will be reconnecting in scenarios (b), (c), (d), or (e) from Figure 1, resulting in either open or closed flux. In each case, sunward flow will be created sunward of the ionospheric projection of the x-line. However, in cases (b) and (d) the field line will be open and connected into the solar wind and will be subject to significant east-west magnetic tension forces; in cases (c) and (e) the field lines will be closed and draped across the dayside magnetopause, with little impetus to move. We might expect quite different evolutions of these differing field lines subsequent to reconnection. In all these cases, however, the flows produced will be sunward on both the sunward and antisunward sides of the x-line, shown as green flow streamlines in Figure 11.

In Figure 1d we have envisaged that the SLR occurs in the northern lobe, and the discussion above has applied to the northern hemisphere ionosphere. If, on the other hand, the reconnection occurs in the southern lobe, then in the northern hemisphere the field line will be opened but connected through the tail into the solar wind in the southern hemisphere. It is unclear how this field line will subsequently evolve, but certainly there is no immediate application of a tension force to make it move sunwards; we have shown possible antisunwards flows away from the x-line by blue streamlines in Figure 11. We note that although the Rankin Inlet radar observes predominantly sunwards flows in the noon sector, at far ranges (around 1,400 km in Figure 10), patches of antisunwards velocities are also seen: these could be the source of the antisunward flow channels seen by DMSP on the nightside, with the boundary between anti/sunwards flows seen by the radar mapping to the ionospheric projection of the x-line.

The result of the patchy and episodic reconnection will be bursty sunwards flows sunward of the x-line, with more complicated flows on the nightside, as suggested by the observations: it was for this reason that Figures 5–8 were shown in order of dayside to nightside traversals of the polar regions by the DMSP spacecraft, with more uniform flows at the dayside and more complicated flows on the nightside. The schematic of Figure 11 shows where vorticity in the convection pattern would give rise to upwards FACs and auroral emissions. We expect that this complicated pattern of flows would evolve with time, and indeed the flow channels and auroral arcs are seen to move about between passes of the DMSP spacecraft. It is probable that the auroral emissions are even evolving during the spacecraft traversal of the polar regions (over approximately 20 min), so the images should not be treated as a "snapshot" of the auroral pattern. There is some indication (e.g., Figure 7) that the dayside and nightside portions of the cusp-aligned arcs may not necessarily join, in which case they could be produced by different mechanisms, maybe the mechanism of Zhang et al. (2020) on the nightside and lobe reconnection on the dayside. On the other hand, this apparent disconnection could be a consequence of motions of the arcs during the traversal of DMSP. Higher temporal resolution auroral imaging would likely cast significant light on the formation and dynamics of the arcs.

4. Conclusions

We have reported the observation of cusp-aligned arcs during periods of near-zero IMF clock angle. Similarly to Zhang et al. (2020), we have shown that these arcs are associated with flow shears in the polar convection pattern. We propose that DLR is first responsible for a significant closure of the magnetosphere, but subsequently complicated lobe reconnection geometries involving open and closed magnetospheric field lines could produce these flow shears. This pattern would evolve with time, but highly similar patterns would be expected in the two hemispheres. We expect that high-cadence (minutes rather than 10s of minutes) imaging of the auroral emissions are required to fully resolve the formation mechanism of the arcs.

Data Availability Statement

The high resolution (1-min) OMNI data used in this study were obtained from the NASA Goddard Space Flight Center Space Physics Data Facility OMNIWeb portal (https://omniweb.gsfc.nasa.gov/form/om_filt_min.html). The Defense Meteorological Satellite Program (DMSP) Special Sensor Ultraviolet Spectrographic Instrument (SSUSI) file type EDR-AUR data were obtained from JHU/APL (http://ssusi.jhuapl.edu, data version 0106, software version 7.0.0, calibration period version E0018). The DMSP Special Sensors-Ions, Electrons, and Scintillation (SSIES) thermal plasma analysis package Topside Ionospheric Plasma Monitor Ion Driftmeter (IDM) data were downloaded from the Coupling, Energetics and Dynamics of Atmospheric Regions (CEDAR) Program Madrigal Database (http://cedar.openmadrigal.org/) using APIs developed by the Open Madrigal Initiative (http://cedar.openmadrigal.org/madrigalDownload). The DMSP SSJ/4 particle detector data were obtained from JHU/APL (http://sd-www.jhuapl.edu/Aurora/dataset_list.html), and processed using software provided (http://sd-www.jhuapl.edu/Aurora/software/index.html). Advanced Magnetosphere and Planetary Electrodynamics Response Experiment (AMPERE) data were obtained from JHU/APL (http://ampere.jhuapl.edu/dataget/index.html) and processed using software provided (http://ampere.jhuapl.edu/).

Acknowledgments
S. E. Milan and J. A. Carter are supported by the Science and Technology Facilities Council (STFC), UK, Grant No. ST/S000429/1. G. E. Bower is supported by an STFC studentship. M. R. Hairston was supported by the National Science Foundation under grant AGS-1929866 and by NASA under Grant 80NSSC20K1071. The work at the Birkeland Centre for Space Science is supported by the Research Council of Norway under contract 223252/F50. BH is supported by the Belgian National Fund for Scientific Research (FNRS). We acknowledge use of NASA/GSFC's Space Physics Data Facility's CDAWeb service (at http://cdaweb.gsfc.nasa.gov), and OMNI data. The DMSP SSJ/4 particle detectors were designed by Dave Hardy of AFRL.

References

Anderson, B., Takahashi, K., & Toth, B. (2000). Sensing global Birkeland currents with Iridium® engineering magnetometer data. *Geophysical Research Letters*, *27*(24), 4045–4048. https://doi.org/10.1029/2000GL000094

Cai, L., Kullen, A., Zhang, Y., Karlsson, T., & Vaivads, A. (2021). DMSP Observations of High-Latitude Dayside Aurora (HiLDA). *Journal of Geophysical Research: Space Physics*, *126*(4), e2020JA028808. https://doi.org/10.1029/2020JA028808

Carter, J., Milan, S., Fear, R., Walach, M.-T., Harrison, Z., Paxton, L., & Hubert, B. (2017). Transpolar arcs observed simultaneously in both hemispheres. *Journal of Geophysical Research: Space Physics*, *122*(6), 6107–6120. https://doi.org/10.1002/2016JA023830

Carter, J., Milan, S., Fogg, A., Paxton, L., & Anderson, B. (2018). The association of high-latitude dayside aurora with NBZ field-aligned currents. *Journal of Geophysical Research: Space Physics*, *123*(5), 3637–3645. https://doi.org/10.1029/2017JA025082

Carter, J., Milan, S., Fogg, A., Sangha, H., Lester, M., Paxton, L., & Anderson, B. (2020). The evolution of long-duration cusp spot emission during lobe reconnection with respect to field-aligned currents. *Journal of Geophysical Research: Space Physics*, *125*, e2020JA027922. https://doi.org/10.1029/2020JA027922

Chamberlain, J. (1961). *Physics of the aurora and airglow*. Academic Press.

Chisham, G., Freeman, M., Coleman, I., Pinnock, M., Hairston, M., Lester, M., & Sofko, G. (2004). Measuring the dayside reconnection rate during an interval of due northward interplanetary magnetic field. *Annales Geophysicae*, *22*(12), 4243–4258. https://doi.org/10.5194/angeo-22-4243-2004

Chisham, G., Lester, M., Milan, S. E., Freeman, M., Bristow, W., Grocott, A., et al. (2007). A decade of the Super Dual Auroral Radar Network (SuperDARN): Scientific achievements, new techniques and future directions. *Surveys in Geophysics*, *28*(1), 33–109. https://doi.org/10.1007/s10712-007-9017-8

Cowley, S. (1981). Magnetospheric and ionospheric flow and the interplanetary magnetic field. In *AGRD the physical basis of the ionosphere in the solar-terrestrial system* (Vol. 295(4–1), pp. 4–14).

Cowley, S., & Lockwood, M. (1992). Excitation and decay of solar wind-driven flows in the magnetosphere-ionosphere system. *Annales Geophysicae*, *10*, 103–115.

Coxon, J., Milan, S., & Anderson, B. (2018). A review of Birkeland current research using AMPERE. *Electric Currents in Geospace and Beyond*, 257–278. https://doi.org/10.1002/9781119324522.ch16

Cumnock, J., & Blomberg, L. (2004). Transpolar arc evolution and associated potential patterns. *Annales Geophysicae*, *22*(4), 1213–1231. https://doi.org/10.5194/angeo-22-1213-2004

Cumnock, J., Sharber, J., Heelis, R., Blomberg, L. G., Germany, G., Spann, J., & Coley, W. (2002). Interplanetary magnetic field control of theta aurora development. *Journal of Geophysical Research*, *107*(A7). SIA–4. https://doi.org/10.1029/2001JA009126

Dungey, J. (1961). Interplanetary magnetic field and the auroral zones. *Physical Review Letters*, *6*(2), 47–48. https://doi.org/10.1103/physrevlett.6.47

Dungey, J. (1963). The structure of the exosphere, or adventures in velocity space. *Geophysics, The Earth's Environment*.

Elphinstone, R., Murphree, J., Hearn, D. J., Heikkila, W., Henderson, M., Cogger, L., & Sandahl, I. (1993). The auroral distribution and its mapping according to substorm phase. *Journal of Atmospheric and Terrestrial Physics*, *55*(14), 1741–1762. https://doi.org/10.1016/0021-9169(93)90142-L

Fairfield, D. (1967). Polar magnetic disturbances and the interplanetary magnetic field. *Space Research*, *VIII*, 107–119.

Fairfield, D., & Cahill, L., Jr. (1966). Transition region magnetic field and polar magnetic disturbances. *Journal of Geophysical Research*, *71*(1), 155–169. https://doi.org/10.1029/jz071i001p00155

Fairfield, D., Lepping, R., Frank, L., Ackerson, K., Paterson, W., Kokubun, S., et al. (1996). Geotail observations of an unusual magnetotail under very northward IMF conditions. *Journal of Geomagnetism and Geoelectricity*, *48*(5), 473–487. https://doi.org/10.5636/jgg.48.473

Fear, R. (2021). The northward IMF magnetosphere. *Magnetospheres in the Solar System*, 293–309. https://doi.org/10.1002/9781119815624.ch19

Fear, R., Milan, S., Carter, J., & Maggiolo, R. (2015). The interaction between transpolar arcs and cusp spots. *Geophysical Research Letters*, *42*(22), 9685–9693. https://doi.org/10.1002/2015GL066194

Fear, R., Milan, S., Maggiolo, R., Fazakerley, A., Dandouras, I., & Mende, S. (2014). Direct observation of closed magnetic flux trapped in the high-latitude magnetosphere. *Science*, *346*(6216), 1506–1510. https://doi.org/10.1126/science.1257377

Frank, L., Craven, J., Burch, J., & Winningham, J. (1982). Polar views of the Earth's aurora with Dynamics Explorer. *Geophysical Research Letters*, *9*(9), 1001–1004. https://doi.org/10.1029/GL009i009p01001

Frey, H. (2007). Localized aurora beyond the auroral oval. *Reviews of Geophysics*, *45*(1). https://doi.org/10.1029/2005RG000174

Frey, H., Mende, S., Immel, T., Fuselier, S., Claflin, E., Gérard, J.-C., & Hubert, B. (2002). Proton aurora in the cusp. *Journal of Geophysical Research*, *107*(A7). SMP–2. https://doi.org/10.1029/2001JA900161

Fujii, R., & Iijima, T. (1987). Control of the ionospheric conductivities on large-scale Birkeland current intensities under geomagnetic quiet conditions. *Journal of Geophysical Research*, *92*(A5), 4505–4513. https://doi.org/10.1029/JA092iA05p04505

Han, D.-S., Feng, H.-T., Zhang, H., Zhou, S., & Zhang, Y. (2020). A new type of polar cap arc observed in the 1500 MLT sector: 1. Northern hemisphere observations. *Geophysical Research Letters*, *47*(20), e2020GL090261. https://doi.org/10.1029/2020GL090261

Hardy, D. A. (1984). Precipitating electron and ion detectors (SSJ/4) for the block 5D/flights 6-10 DMSP satellites: Calibration and data presentation. *Rep. AFGL-TR-84-0317*.

Hones, E., Jr., Craven, J., Frank, L., Evans, D., & Newell, P. (1989). The horse-collar aurora: A frequent pattern of the aurora in quiet times. *Geophysical Research Letters*, *16*(1), 37–40. https://doi.org/10.1029/GL016i001p00037

Hosokawa, K., Kullen, A., Milan, S., Reidy, J., Zou, Y., Frey, H. U., et al. (2020). Aurora in the polar cap: A review. *Space Science Reviews*, *216*(1), 15. https://doi.org/10.1007/s11214-020-0637-3

Huang, C.-S., Foster, J., Song, P., Sofko, G., Frank, L., & Paterson, W. (2002). Geotail observations of magnetospheric midtail during an extended period of strongly northward interplanetary magnetic field. *Geophysical Research Letters*, *29*(4), 15–1. https://doi.org/10.1029/2001GL014170

Huang, C.-S., Sofko, G., Koustov, A., Andre, D., Ruohoniemi, J., Greenwald, R., & Hairston, M. (2000). Evolution of ionospheric multicell convection during northward interplanetary magnetic field with $|B_z/B_y| > 1$. *Journal of Geophysical Research*, *105*(A12), 27095–27107. https://doi.org/10.1029/2000JA000163

Iijima, T., & Potemra, T. (1976). The amplitude distribution of field-aligned currents at northern high latitudes observed by Triad. *Journal of Geophysical Research*, *81*(13), 2165–2174. https://doi.org/10.1029/JA081i013p02165

Iijima, T., Potemra, T., Zanetti, L., & Bythrow, P. (1984). Large-scale Birkeland currents in the dayside polar region during strongly northward IMF: A new Birkeland current system. *Journal of Geophysical Research*, *89*(A9), 7441–7452. https://doi.org/10.1029/JA089iA09p07441

Imber, S., Milan, S., & Hubert, B. (2006). The auroral and ionospheric flow signatures of dual lobe reconnection. *Annales Geophyiscae*, *24*(11), 3115–3129. https://doi.org/10.5194/angeo-24-3115-2006

Imber, S., Milan, S., & Hubert, B. (2007). Observations of significant flux closure by dual lobe reconnection. *Annales Geophysicae*, *25*, 1617–1627. https://doi.org/10.5194/angeo-25-1617-2007

King, J., & Papitashvili, N. (2005). Solar wind spatial scales in and comparisons of hourly Wind and ACE plasma and magnetic field data. *Journal of Geophysical Research*, *110*(A2). https://doi.org/10.1029/2004JA010649

Kullen, A. (2012). Transpolar arcs: Summary and recent results. Auroral phenomenology and magnetospheric processes: Earth and other planets. *Geophysical Monograph Series*, *197*, 69–80. https://doi.org/10.1029/2011GM001183

Kullen, A., Brittnacher, M., Cumnock, J., & Blomberg, L. (2002). Solar wind dependence of the occurrence and motion of polar auroral arcs: A statistical study. *Journal of Geophysical Research*, *107*(A11), 13–1. https://doi.org/10.1029/2002JA009245

Lockwood, M., & Cowley, S. (1992). Ionospheric convection and the substorm cycle. *Proceedings of the International Congress of Speleology*, 99–109.

Lu, G., Li, W., Raeder, J., Deng, Y., Rich, F., Ober, D., et al. (2011). Reversed two-cell convection in the northern and southern hemispheres during northward interplanetary magnetic field. *Journal of Geophysical Research*, *116*(A12). https://doi.org/10.1029/2011JA017043

Marcucci, M., Coco, I., Ambrosino, D., Amata, E., Milan, S., Bavassano Cattaneo, M., & Retinò, A. (2008). Extended SuperDARN and IMAGE observations for northward IMF: Evidence for dual lobe reconnection. *Journal of Geophysical Research*, *113*(A2). https://doi.org/10.1029/2007JA012466

Milan, S. (2004). A simple model of the flux content of the distant magnetotail. *Journal of Geophysical Research*, *109*(A7). https://doi.org/10.1029/2004JA010397

Milan, S. (2013). Modeling Birkeland currents in the expanding/contracting polar cap paradigm. *Journal of Geophysical Research: Space Physics*, *118*(9), 5532–5542. https://doi.org/10.1002/jgra.50393

Milan, S., Carter, J., Bower, G., Imber, S., Paxton, L., Anderson, B., et al. (2020). Dual-lobe reconnection and horse-collar auroras. *Journal of Geophysical Research: Space Physics*, *125*(10), e2020JA028567. https://doi.org/10.1029/2020JA028567

Milan, S., Carter, J., & Hubert, B. (2020). Probing the magnetic structure of a pair of transpolar arcs with a solar wind pressure step. *Journal of Geophysical Research: Space Physics*, *125*(2), e2019JA027196. https://doi.org/10.1029/2019ja027196

Milan, S., Clausen, L., Coxon, J., Carter, J., Walach, M.-T., Laundal, K., et al. (2017). Overview of solar wind–magnetosphere–ionosphere–atmosphere coupling and the generation of magnetospheric currents. *Space Science Reviews*, *206*(1–4), 547–573. https://doi.org/10.1007/s11214-017-0333-0

Milan, S., Hubert, B., & Grocott, A. (2005). Formation and motion of a transpolar arc in response to dayside and nightside reconnection. *Journal of Geophysical Research*, *110*(A1). https://doi.org/10.1029/2004JA010835

Milan, S., Hutchinson, J., Boakes, P., & Hubert, B. (2009). Influences on the radius of the auroral oval. *Annales Geophysicae*, *27*(7), 2913–2924. https://doi.org/10.5194/angeo-27-2913-2009

Milan, S., Lester, M., Cowley, S., & Brittnacher, M. (2000a). Convection and auroral response to a southward turning of the IMF: Polar UVI, CUTLASS, and IMAGE signatures of transient magnetic flux transfer at the magnetopause. *Journal of Geophysical Research*, *105*(A7), 15741–15755. https://doi.org/10.1029/2000JA900022

Milan, S., Lester, M., Cowley, S., & Brittnacher, M. (2000b). Dayside convection and auroral morphology during an interval of northward interplanetary magnetic field. *Annales Geophysicae*, *18*(4), 436–444. https://doi.org/10.1007/s00585-000-0436-9

Milan, S., Provan, G., & Hubert, B. (2007). Magnetic flux transport in the Dungey cycle: A survey of dayside and nightside reconnection rates. *Journal of Geophysical Research*, *112*(A1). https://doi.org/10.1029/2006JA011642

Murphree, J., Anger, C., & Cogger, L. (1982). The instantaneous relationship between polar cap and oval auroras at times of northward interplanetary magnetic field. *Canadian Journal of Physics*, *60*(3), 349–356. https://doi.org/10.1139/p82-047

Ness, N., Scearce, C., & Cantarano, S. (1967). Probable observations of the geomagnetic tail at 10^3 Earth radii by Pioneer 7. *Journal of Geophysical Research*, *72*(15), 3769–3776. https://doi.org/10.1029/jz072i015p03769

Paxton, L., Meng, C.-I., Fountain, G., Ogorzalek, B., Darlington, E., Gary, S., et al. (1992). Special sensor ultraviolet spectrographic imager: An instrument description. *Instrumentation for planetary and terrestrial atmospheric remote sensing*, *1745*, 2–15. https://doi.org/10.1117/12.60595

Paxton, L., Schaefer, R., Zhang, Y., & Kil, H. (2017). Far ultraviolet instrument technology. *Journal of Geophysical Research: Space Physics*, *122*(2), 2706–2733. https://doi.org/10.1002/2016JA023578

Paxton, L., & Zhang, Y. (2016). Far ultraviolet imaging of the aurora. In *Space weather fundamentals* (pp. 213–244). CRC Press. https://doi.org/10.1201/9781315368474-14

Paxton, L., Zhang, Y., Kil, H., & Schaefer, R. (2021). Exploring the upper atmosphere: Using optical remote sensing. *Upper Atmosphere Dynamics and Energetics*, 487–522. https://doi.org/10.1002/9781119815631.ch23

Pinnock, M., Rodger, A., Dudeney, J., Rich, F., & Baker, K. (1995). High spatial and temporal resolution observations of the ionospheric cusp. *Annales Geophysicae*, *13*(9), 919–925. https://doi.org/10.1007/s00585-995-0919-9

Provan, G., Yeoman, T. K., & Milan, S. E. (1998). CUTLASS Finland radar observations of the ionospheric signatures of flux transfer events and the resulting plasma flows. *Annales Geophysicae*, *16*(11), 1411–1422. https://doi.org/10.1007/s00585-998-1411-0

Reiff, P., & Burch, J. (1985). IMF by-dependent plasma flow and Birkeland currents in the dayside magnetosphere: 2. A global model for northward and southward IMF. *Journal of Geophysical Research*, *90*(A2), 1595–1609. https://doi.org/10.1029/JA090iA02p01595

Rich, F., & Hairston, M. (1994). Large-scale convection patterns observed by DMSP. *Journal of Geophysical Research*, *99*(A3), 3827–3844. https://doi.org/10.1029/93JA03296

Ruohoniemi, J., & Baker, K. (1998). Large-scale imaging of high-latitude convection with super dual auroral radar network HF radar observations. *Journal of Geophysical Research*, *103*(A9), 20797–20811. https://doi.org/10.1029/98JA01288

Siscoe, G. L., Farrugia, C. J., & Sandholt, P. E. (2011). Comparison between the two basic modes of magnetospheric convection. *Journal of Geophysical Research*, *116*(A5). https://doi.org/10.1029/2010JA015842

Song, P., DeZeeuw, D., Gombosi, T., Groth, C., & Powell, K. (1999). A numerical study of solar wind-magnetosphere interaction for northward interplanetary magnetic field. *Journal of Geophysical Research*, *104*(A12), 28361–28378. https://doi.org/10.1029/1999JA900378

Song, P., & Russell, C. (1992). Model of the formation of the low-latitude boundary layer for strongly northward interplanetary magnetic field. *Journal of Geophysical Research*, *97*(A2), 1411–1420. https://doi.org/10.1029/91JA02377

Thomas, E. G., & Shepherd, S. G. (2018). Statistical patterns of ionospheric convection derived from mid-latitude, high-latitude, and polar SuperDARN HF radar observations. *Journal of Geophysical Research: Space Physics*, *123*(4), 3196–3216. https://doi.org/10.1002/2018JA025280

Waters, C., Anderson, B., & Liou, K. (2001). Estimation of global field aligned currents using the Iridium® system magnetometer data. *Geophysical Research Letters*, *28*(11), 2165–2168. https://doi.org/10.1029/2000GL012725

Wild, J., Cowley, S. W. H., Davies, J., Khan, H., Lester, M., Milan, S., et al. (2001). First simultaneous observations of flux transfer events at the high-latitude magnetopause by the Cluster spacecraft and pulsed radar signatures in the conjugate ionosphere by the CUTLASS and EISCAT radars. *Annales Geophysicae*, *19*(10/12), 1491–1508. https://doi.org/10.5194/angeo-19-1491-2001

Woch, J., & Lundin, R. (1992). Magnetosheath plasma precipitation in the polar cusp and its control by the interplanetary magnetic field. *Journal of Geophysical Research*, *97*(A2), 1421–1430. https://doi.org/10.1029/91JA02487

Wolfe, J., Silva, R., McKibbin, D., & Mason, R. (1967). Preliminary observations of a geomagnetospheric wake at 1000 Earth radii. *Journal of Geophysical Research*, *72*(17), 4577–4581. https://doi.org/10.1029/JZ072i017p04577

Zhang, Q.-H., Zhang, Y.-L., Wang, C., Lockwood, M., Yang, H.-G., Tang, B.-B., et al. (2020). Multiple transpolar auroral arcs reveal insight about coupling processes in the Earth's magnetotail. *Proceedings of the National Academy of Sciences*, *117*(28), 16193–16198. https://doi.org/10.1073/pnas.2000614117

Zhang, Q.-H., Zhang, Y.-L., Wang, C., Oksavik, K., Lyons, L., Lockwood, M., et al. (2021). A space hurricane over the Earth's polar ionosphere. *Nature Communications*, *12*(1), 1–10. https://doi.org/10.1038/s41467-021-21459-y

Zhang, Y., Paxton, L., Zhang, Q.-H., & Xing, Z. (2016). Polar cap arcs: Sun-aligned or cusp-aligned? *Journal of Atmospheric and Solar-Terrestrial Physics*, *146*, 123–128. https://doi.org/10.1016/j.jastp.2016.06.001

Zhu, L., Schunk, R., & Sojka, J. (1997). Polar cap arcs: A review. *Journal of Atmospheric and Solar-Terrestrial Physics*, *59*(10), 1087–1126. https://doi.org/10.1016/S1364-6826(96)00113-7